

# Multiplexed Quantification of Nucleic Acids with Large Dynamic Range Using Multivolume Digital RT-PCR on a Rotational SlipChip Tested with HIV and Hepatitis C Viral Load

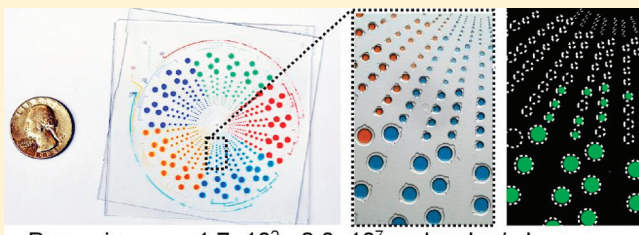
Feng Shen,<sup>#,†</sup> Bing Sun,<sup>#</sup> Jason E. Kreutz,<sup>#</sup> Elena K. Davydova,<sup>#</sup> Wenbin Du,<sup>#,‡</sup> Poluru L. Reddy,<sup>‡</sup> Loren J. Joseph,<sup>‡</sup> and Rustem F. Ismagilov<sup>\*,#,§</sup>

<sup>#</sup>Department of Chemistry and Institute for Biophysical Dynamics, The University of Chicago, 929 East 57th Street, Chicago, Illinois 60637, United States

<sup>‡</sup>Department of Pathology, University of Chicago Medical Center, 5481 S. Maryland Avenue, Chicago, Illinois 60637, United States

**S** Supporting Information

**ABSTRACT:** In this paper, we are working toward a problem of great importance to global health: determination of viral HIV and hepatitis C (HCV) loads under point-of-care and resource limited settings. While antiretroviral treatments are becoming widely available, viral load must be evaluated at regular intervals to prevent the spread of drug resistance and requires a quantitative measurement of RNA concentration over a wide dynamic range (from 50 up to  $10^6$  molecules/mL for HIV and up to  $10^8$  molecules/mL for HCV). “Digital” single molecule measurements are attractive for quantification, but the dynamic range of such systems is typically limited or requires excessive numbers of compartments. Here we designed and tested two microfluidic rotational SlipChips to perform multivolume digital RT-PCR (MV digital RT-PCR) experiments with large and tunable dynamic range. These designs were characterized using synthetic control RNA and validated with HIV viral RNA and HCV control viral RNA. The first design contained 160 wells of each of four volumes (125 nL, 25 nL, 5 nL, and 1 nL) to achieve a dynamic range of  $5.2 \times 10^2$  to  $4.0 \times 10^6$  molecules/mL at 3-fold resolution. The second design tested the flexibility of this approach, and further expanded it to allow for multiplexing while maintaining a large dynamic range by adding additional wells with volumes of 0.2 nL and 625 nL and dividing the SlipChip into five regions to analyze five samples each at a dynamic range of  $1.8 \times 10^3$  to  $1.2 \times 10^7$  molecules/mL at 3-fold resolution. No evidence of cross-contamination was observed. The multiplexed SlipChip can be used to analyze a single sample at a dynamic range of  $1.7 \times 10^2$  to  $2.0 \times 10^7$  molecules/mL at 3-fold resolution with limit of detection of 40 molecules/mL. HIV viral RNA purified from clinical samples were tested on the SlipChip, and viral load results were self-consistent and in good agreement with results determined using the Roche COBAS AmpliPrep/COBAS TaqMan HIV-1 Test. With further validation, this SlipChip should become useful to precisely quantify viral HIV and HCV RNA for high-performance diagnostics in resource-limited settings. These microfluidic designs should also be valuable for other diagnostic and research applications, including detecting rare cells and rare mutations, prenatal diagnostics, monitoring residual disease, and quantifying copy number variation and gene expression patterns. The theory for the design and analysis of multivolume digital PCR experiments is presented in other work by Kreutz et al.



Dynamic range  $1.7 \times 10^2$  -  $2.0 \times 10^7$  molecules/mL  
Detection limit 40 molecules/mL

## INTRODUCTION

This paper describes a rotational SlipChip to quantify RNA with large dynamic range by using multivolume digital RT-PCR (MV digital RT-PCR). Quantitative detection of RNA provides valuable information for study of gene expression<sup>1,2</sup> and has the potential to improve evaluation of diseases (including stroke,<sup>3</sup> leukemia,<sup>4</sup> and prostate cancer<sup>5</sup>), analysis of graft rejection in transplantation,<sup>6</sup> and vaccine development.<sup>7,8</sup> Quantification of viral RNA has also become increasingly significant in monitoring the progression of viral infection and efficiency of the applied treatment. One such instance is in the treatment of HIV: more than 33 million people worldwide are living with HIV, and a large number of them are in developing countries and resource-limited

areas.<sup>9</sup> First-line antiretroviral treatment is becoming widely available, and it greatly increases both the duration and quality of life of HIV patients. However, this first-line treatment begins to fail as the virus mutates and develops drug resistance. In order to stop the global spread of drug resistance and provide proper treatment for patients, it is critical to evaluate the HIV viral load at regular intervals (every 3 to 4 months) after the initial treatment is shown to be effective. Moreover, HIV viral load measurement is a particularly useful tool for diagnosing and evaluating the status of HIV infection in children under age 18 months,<sup>10</sup> as persisting

Received: June 28, 2011

Published: October 13, 2011

maternal antibodies can cause false positive result in the HIV antibody test.

The hepatitis C virus (HCV) infection is also a significant global healthcare burden, as it has been identified as one of the major causes of liver disease and is one of the most common coinfections of HIV.<sup>11</sup> Recent breakthroughs in HCV treatments, such as the approval of HCV drugs from Merck and Vertex by the US Food and Drug Administration (FDA), generated excitement,<sup>12,13</sup> but the HCV viral load may still need to be carefully monitored to determine the effectiveness of the treatment. The viral load for chronic HCV ranges from 50 000 to 5 million international units per mL (IU/mL),<sup>14</sup> while for patients responding to antiviral treatment it will be significantly lower.<sup>15</sup> A successful treatment should result in undetectable levels of HCV viral RNA, requiring HCV viral load measurements capable of a wide dynamic range.

Currently, real time quantitative RT-PCR is the gold standard for monitoring viral load for HIV, HCV, and other viral infections. However, this test is cost-prohibitive under resource-limited settings and usually requires multiple instruments, highly skilled technicians, and isolated rooms to prevent contamination; therefore, it is still not accessible to patients in resource-limited settings. Moreover, the efficiency of RT-PCR, the quality of sample and selection of targets, and the methods for interpretation of the data have brought up increasing concerns for the accuracy of quantifying RNA using RT-PCR.<sup>16,17</sup> While a dipstick device has been developed that provides semiquantitative measurements of HIV viral load after amplification in resource-limited settings,<sup>18</sup> no quantitative test exists to resolve a 3-fold ( $0.5 \log_{10}$ ) change in HIV RNA viral load, which is considered to be clinically significant.<sup>19,20</sup> Digital PCR is a method that performs quantitative analysis of nucleic acids by detecting single molecule of DNA or RNA and can provide an absolute count of the nucleic acid copy number with potentially higher accuracy compared to real time PCR.<sup>21,22</sup> Digital PCR has been previously demonstrated on various platforms, including well plates,<sup>22</sup> pneumatically controlled integrated microfluidic systems,<sup>23,24</sup> microdroplets,<sup>25–27</sup> spinning disk,<sup>28</sup> and Openarray.<sup>29</sup> However, most of these methods still rely on complex instruments and chips to generate a large number of small-volume reaction compartments which are required for digital PCR.

SlipChip is a microfluidic platform that can manipulate liquid samples from picoliter-to-microliter scales by relative movement of different plates without the need for complex control systems.<sup>30</sup> The SlipChip has been previously used for multiplex PCR,<sup>31</sup> digital PCR,<sup>32</sup> and digital isothermal amplification (RPA).<sup>33</sup> Instead of using wells of uniform size, using wells of multiple volumes to achieve the same dynamic range can significantly reduce the total number of wells and increase the spacing among wells to simplify imaging and downstream analysis. The mathematical approach for experimental design and statistical analysis for multivolume digital PCR (MV digital PCR) has been characterized using DNA in an accompanying study.<sup>34</sup>

Here, we describe a SlipChip platform for quantitative analysis of RNA with large dynamic range by MV digital RT-PCR. As RNA is more susceptible to degradation under the testing environment and requires a reverse transcription step for downstream PCR amplification, it was not obvious whether the multivolume digital approach would apply to RT-PCR analysis of RNA, and therefore we first characterized this SlipChip with a serial dilution of a synthetic control RNA molecule of 906 nt.

nucleotides (906 nt). We also describe a second design of the platform that can maintain a large dynamic range for five samples simultaneously, allowing for multiplexed experiments. We validated this multiplexed system by using HCV control viral RNA and HIV viral RNA together with internal controls. We also showed the potential to use multivolume designs to quantify HIV viral load at a large dynamic range by quantifying purified HIV viral RNA from clinical patients' samples.

## RESULTS AND DISCUSSION

We first characterized the performance of digital RT-PCR in a multivolume digital SlipChip (design 1, Table 1) with a large dynamic range that is required for viral load testing. This SlipChip contained four different volumes (1 nL, 5 nL, 25 nL, 125 nL) with 160 wells each (Figure 1A) for a theoretical dynamic range (lower dynamic range, LDR, to upper limit of quantification, ULQ) of  $5.2 \times 10^2$  to  $4.0 \times 10^6$  molecules/mL at 3-fold resolution and a lower detection limit (LDL) of  $1.2 \times 10^2$  molecules/mL in the final RT-PCR mixture. The LDR corresponds to the lowest concentration that can be resolved from a 3- or 5-fold higher concentration; the ULQ is the concentration that has a 95% chance of generating at least one negative well and is equal to the concentration calculated from three negative wells; the LDL is the concentration that has a 95% chance of generating at least one positive well and is equal to the concentration calculated from three positive wells.<sup>34</sup> Continuous fluidic paths are generated by partially overlapping the wells in the top plate and the wells in the bottom plate (Figure 1B,E). The design of this SlipChip follows the general principles of dead-end filling<sup>35</sup> for complete filling of aqueous reagents (Figure 1C,F). After complete loading, the top plate is slipped (rotated) clockwise by  $\sim 8^\circ$  to break the fluidic path and overlay the wells filled with solution with the wells in the facing plate used to control thermal expansion<sup>31</sup> (Figure 1D,G). The SlipChip is then placed on a flat *in situ* adaptor for thermal cycling.

The theory for design and analysis of this multivolume SlipChip are described in detail and validated by using digital PCR for DNA in an accompanying study.<sup>34</sup> In brief, concentrations were calculated based on Most Probable Number (MPN) theory<sup>36–39</sup> by combining the results from each volume ( $i = 1, 2, 3, 4$ ) in eq 1 and solving for  $\lambda$  (concentration, molecules/mL), where  $n_i$  is the total number of wells at each volume,  $b_i$  is the number of negative wells at that volume, and  $v_i$  is the well volume (mL). Combining results allows for more precise identification of the "most probable" concentration and also improves the confidence interval. To find the confidence interval, the standard deviation,  $\sigma$ , for  $\ln(\lambda)$  is determined using eq 2, which was derived based on the Fisher information.<sup>34,39</sup>

$$\sum_{i=1}^m n_i v_i = \sum_{i=1}^m \frac{(n_i - b_i)v_i}{(1 - e^{-v_i\lambda})} \quad (1)$$

$$\sigma = \frac{1}{\sqrt{\lambda^2 \sum_{i=1}^m \frac{v_i^2 n_i}{e^{v_i \lambda}} - 1}} \quad (2)$$

To validate the performance of the multivolume SlipChip with RNA, we performed digital RT-PCR using a six order-of-magnitude serial dilution of synthetic control RNA template (906 nt). This control RNA was synthesized from a control plasmid

**Table 1.** Summary of Detection Limit and Dynamic Range for Multivolume SlipChip in the RT-PCR Mix

	number of wells						molecules/mL				
	625 nL	125 nL	25 nL	5 nL	1 nL	0.2 nL	LDL <sup>a</sup>	LDR-5 <sup>b</sup>	LDR-3 <sup>c</sup>	ULQ-3 <sup>d</sup>	total volume per sample, $\mu\text{L}$
design 1	0	160	160	160	160	0	$1.2 \times 10^2$	$2.0 \times 10^2$	$5.2 \times 10^2$	$4.0 \times 10^6$	25
design 2A	16	32	32	32	32	32	$2.0 \times 10^2$	$4.0 \times 10^2$	$1.8 \times 10^3$	$1.2 \times 10^7$	15
design 2B	80	160	160	160	160	160	67	$1.7 \times 10^2$	$2.0 \times 10^7$	75	

<sup>a</sup> Lower detection limit, the concentration that has a 95% chance of generating at least one positive well, corresponds to concentration calculated from three positive wells. <sup>b</sup> Lower dynamic range, 5-fold resolution, lowest concentration that can be resolved from a 5-fold higher concentration. <sup>c</sup> Lower dynamic range, 3-fold resolution, lowest concentration that can be resolved from a 3-fold higher concentration. <sup>d</sup> Upper limit of quantification, 3-fold resolution, the concentration that has a 95% chance of generating at least one negative well, corresponds to the concentration calculated from three negative wells. See Kreutz et al.<sup>34</sup> for further details of the theory.

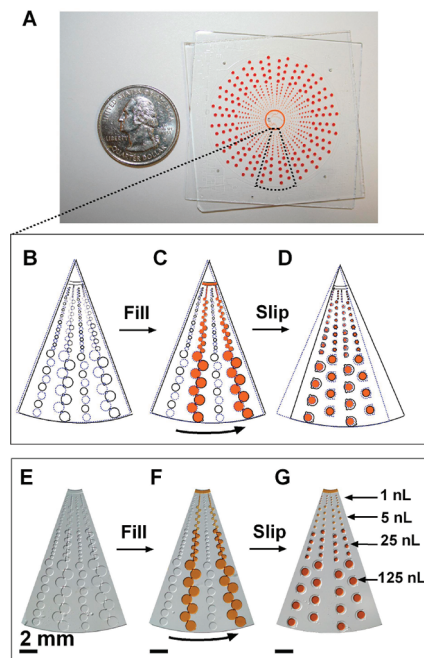


**Figure 1.** Rotational multivolume SlipChip (well volumes: 1 nL, 5 nL, 25 nL, 125 nL). (A) Bright field image of the rotational SlipChip after slipping to form isolated compartments, shown next to a U.S. quarter. (B–D) Schematics and (E–G) bright field microphotograph show (B, E) the assembled rotational SlipChip. (C, F) The SlipChip filled with food dye after dead-end filling. (D, G) The SlipChip after rotational slipping: 640 aqueous droplets of four different volumes (160 wells with volumes of 1 nL, 5 nL, 25 nL, 125 nL each) were formed simultaneously. In the schematics, blue dotted lines indicate features in the top plate, and black solid lines represent the features in the bottom plate.

and purified by using a commercial purification kit (see Experimental Section in Supporting Information). The concentration of the stock solution of control RNA was measured spectrophotometrically by NanoDrop to be  $\sim 1.8 \text{ ng}/\mu\text{L}$ , corresponding to  $\sim 4.1 \times 10^{12} \text{ molecules/mL}$ , which is not perfectly accurate and contains background noise. Using the SlipChip and through statistical analysis<sup>34</sup> of all MV digital RT-PCR results (Figure 3), we obtained a nominal real concentration of the control RNA in solution,  $2.2 \times 10^{12} \text{ molecules/mL}$  and used this value as the true concentration of all MV digital RT-PCR results reported in Figure 3. A RT-PCR master mix containing EvaGreen SuperMix, RT-transcriptase, bovine serum albumin (BSA), and primers was mixed with the RNA template solution. EvaGreen,

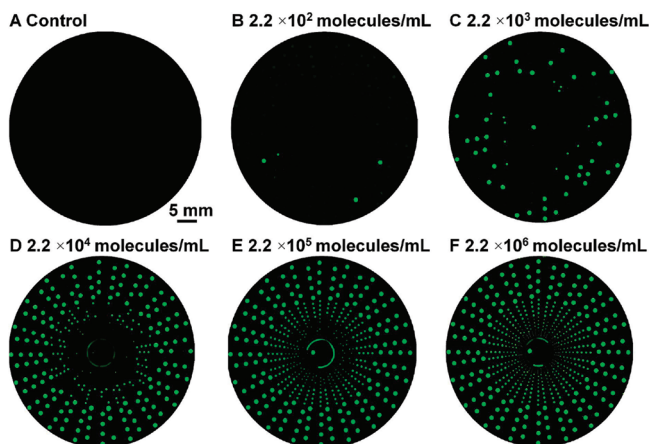


**Figure 2.** End-point fluorescence images of multivolume digital RT-PCR performed on a rotational SlipChip for synthetic RNA template at five different concentrations. (A) Control, containing no RNA template. (B–F) Serial dilution of 906 nt RNA template from  $2.2 \times 10^2$  to  $2.2 \times 10^6$  molecules/mL in the RT-PCR mix.

an intercalating dye, was used for end-point fluorescent imaging after thermal cycling (Figure 2).

No false positives were observed after amplification in four negative control experiments, as there was no significant increase of fluorescent intensity in wells (Figure 2A). As the concentration of RNA template increased (the dilution factor decreased), the fraction of positive wells in each set of individual volumes was counted and the concentration of template in the RT-PCR mix was calculated as described above (Figure 2B–F). The glass SlipChip was reused after being thoroughly cleaned with piranha acid (3:1 sulfuric acid:hydrogen peroxide), plasma cleaned, and resilanized with dichlorodimethylsilane (see Experimental Section in Supporting Information). Four to five experiments were performed for each concentration of template, and the calculated concentration of template RNA showed good agreement within the expected statistical distribution at each concentration and scaled linearly with the expected concentration (Figure 3A). The results at the concentrations of  $2.2 \times 10^6$ ,  $2.2 \times 10^5$ ,  $2.2 \times 10^4$ ,  $2.2 \times 10^3$ ,  $2.2 \times 10^2$ , and  $7.3 \times 10^1$  molecules/mL in the RT-PCR mix were used to estimate an initial stock concentration of control RNA of approximately  $2.2 \times 10^{12}$  molecules/mL. The experimental results across the concentrations agree well with the theoretically predicted<sup>34</sup> distribution (Figure 3A,B). Of the 26 experiments, 19 fall within the 95% confidence interval and 22 fall

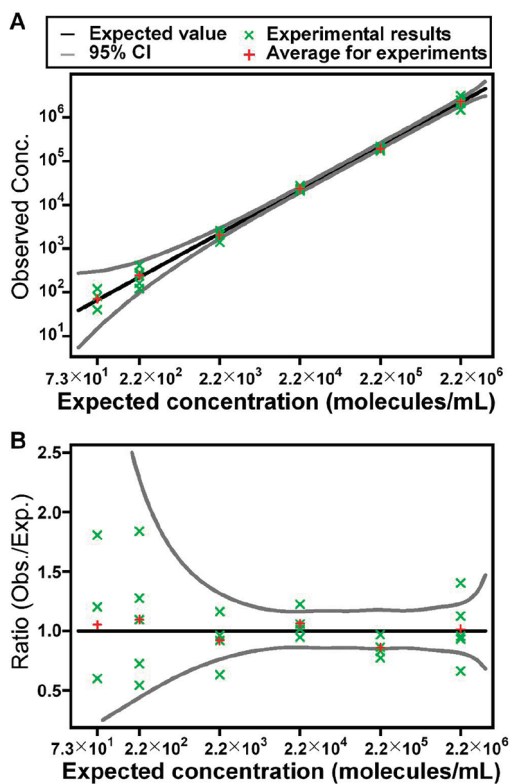


**Figure 3.** Performance of digital RT-PCR with synthetic RNA template on the multivolume SlipChip over a 4  $\log_{10}$  dynamic range, comparing the expected concentration of RNA in RT-PCR mix to (A) the observed concentration, and (B) the ratio of the observed/expected concentration. Individual experimental results (green crosses) and average results (red crosses) for concentration were plotted against the dilution level of the RNA stock solution. Four to five experiments were performed at each concentration, and some experimental results are overlapping. The experimental results show a linear relationship with the dilution level and fit within the expected distribution. The experimental results were used to estimate an initial stock concentration, whose distribution was then fit to the dilution level to provide the expected value (black curve) and 95% confidence interval (gray curves).

within the 99% confidence interval. The confidence interval is based only on the theoretical distribution, so it is reasonable that the experimental distribution is a little broader due to experimental variations such as dilution errors and RNA degradation.

Over the dynamic range of the device, the contribution of wells with different volumes to the calculated concentration varies and is approximated in Figure 4A. As the concentration of control RNA template increases (the dilution decreases), the major contribution to the calculated final concentration shifts from wells of large volume (125 nL) to wells of medium volume (25 nL and 5 nL) and then to wells of small volume (1 nL). The percent that the result from each volume contributes to  $\sigma$  (eq 2) serves as an estimate of the relative contribution of that volume to the concentration determined by all volumes on the entire chip. The concentration calculated from analysis of positive and negative wells of each of the volumes on the individual SlipChip was self-consistent and was consistent with the calculated concentration determined by combining all wells with different volumes (Figure 4B). This result indicates that multivolume digital approach is fully compatible with analysis of RNA by RT-PCR.

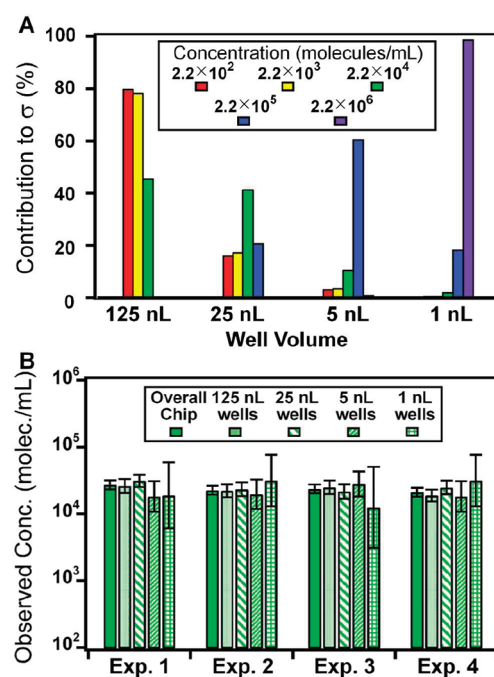


**Figure 4.** (A) For each dilution, the approximate contributions of the results from each well volume toward calculating the final concentration were calculated based on the contributions of each volume to the standard deviation,  $\sigma$  (eq 2). (B) Concentration of RNA template calculated from the overall chip (combining all well volumes, solid bars) and individual volumes (patterned bars) is self-consistent on the MV digital RT-PCR SlipChip. Four experiments were performed with  $2.2 \times 10^4$  molecules/mL of control RNA template (906 nt) in the RT-PCR mix.

To test whether multiplexing can be easily incorporated into the SlipChip while maintaining the high dynamic range, we modified the design of the multivolume SlipChip by adding two additional volumes (Table 1, design 2A): 0.2 nL (160 wells) and 625 nL (80 wells). When the rotational chip is split into five sections to quantify five different analytes, the 0.2 nL wells extend the upper limit of quantification with 3-fold resolution to  $1.2 \times 10^7$  molecules/mL in the RT-PCR mix, and the 625 nL wells maintain a reasonable lower detection limit of  $2.0 \times 10^2$  molecules/mL and lower dynamic range with 3-fold resolution at  $1.8 \times 10^3$  molecules/mL in the RT-PCR mix (Figure 5A). The higher upper limit of quantification is required to quantify HCV viral RNA, and the lower dynamic range and lower detection limit are required for the HIV viral load test. Five different solutions can be introduced into the SlipChip simultaneously (Figure 5A) for multiplexed analysis.

As HCV is one of the most common coinfections for HIV patients, we first validated this multiplex SlipChip with five-plex panel: measurement of HIV viral RNA, measurement of HCV control viral RNA, a negative control for HIV, a negative control for HCV, and measurement of 906 nt control RNA in HCV sample for quantification of sample recovery rate (Figure 5B,C). The 906 nt control RNA was the same one characterized by using digital RT-PCR on the SlipChip (design 1; see Figure 1). HIV viral RNA was purified from an archived sample of plasma containing HIV (viral RNA estimated to be  $\sim 1.5 \times 10^6$  molecules/mL) from a deidentified patient sample, and HCV control viral RNA was purified from a commercial sample containing control HCV virus (25 million IU/mL, OptiQuant-S

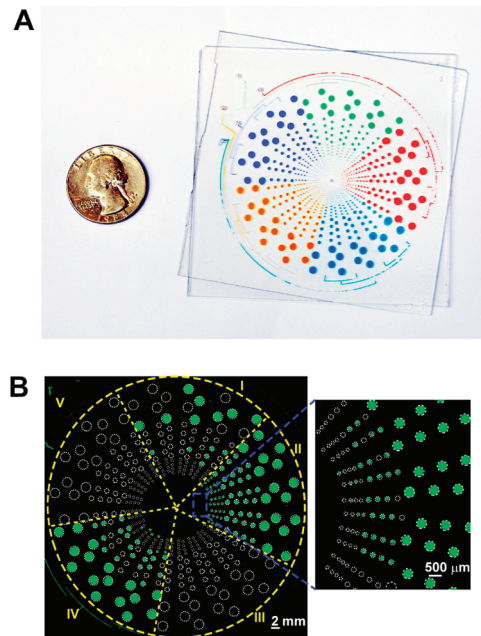


**Figure 5.** A SlipChip for multiplexed, multivolume digital RT-PCR with high dynamic range. (A) A photograph of a multiplex device for up to five samples corresponding to designs 2A and 2B in Table 1 with a total of 80 wells of 625 nL, 160 wells of 125 nL, 160 wells of 25 nL, 160 wells of 5 nL, 160 wells of 1 nL, and 160 wells of 0.2 nL. (B) Fluorescent photograph of a multiplexed digital RT-PCR detection panel: (I) measurement of internal control of 906 nt RNA template in HCV sample; (II) HCV control viral RNA measurement; (III) negative control for HIV (HIV primers with no loaded HIV RNA template); (IV) HIV viral RNA measurement; (V) negative control for HCV (HCV primers with no loaded HCV RNA template). Inset shows an amplified area from HCV viral load test.

HCV Quantification Panel, Acrometrix) using the iPrep purification instrument (see Experimental Section in Supporting Information). As the final elution volume of purified nucleic acid is generally smaller than the starting volume of plasma, there is a concentrating effect on viral RNA after sample purification. To characterize this concentrating effect, the 906 nt control RNA with known concentration was added to the lysed plasma and was quantified again after sample preparation. The ratio of the concentration of 906 nt control RNA after/before sample preparation is defined as the concentrating factor. The concentrating factors after sample purification were approximately 6.6 for HIV viral RNA and approximately 4.5 for HCV control viral RNA. Primers for HIV and HCV were selected from previous publications.<sup>40,41</sup> Only one pair of primers was added to each sample, and the experiment was repeated six times. In those six experiments, no false positives were observed in either HIV or HCV negative control panels after thermal cycling, and no cross-contamination was observed among different panels. From these six experiments, the average calculated concentration of HIV viral RNA after purification was  $7.9 \times 10^6$  molecules/mL with standard deviation of  $2.5 \times 10^6$  molecules/mL, corresponding to  $1.2 \times 10^6$  molecules/mL with standard deviation of  $3.7 \times 10^5$  molecules/mL in the original plasma sample. The average concentration of HCV control viral RNA after purification was  $1.0 \times 10^8$  molecules/mL with standard deviation of  $4.4 \times 10^7$  molecules/mL, corresponding to  $2.3 \times 10^7$  molecules/mL with standard deviation of  $9.7 \times 10^6$  molecules/mL in the original

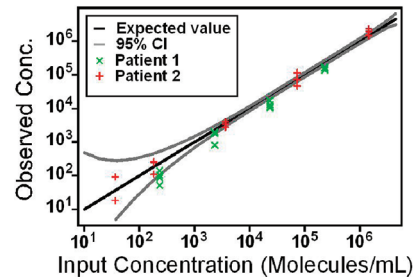


**Figure 6.** Multivolume digital RT-PCR for quantification of HIV viral load in two patients' samples. Input concentration was calculated from a single clinical measurement for each patient using the Roche CAP/CTM v2.0 system and was assumed to be the true concentration. Each concentration was measured at least four times, and each individual experiment is plotted as single point on the graph. The black solid line is the predicted concentration based on the assumption that the clinical measurement gave a true concentration. The gray solid lines were calculated using MPN theory<sup>34</sup> and represent the 95% confidence interval for the predicted concentration.

control plasma sample. There is no universal conversion factor from international units to copy number for HCV viral load; it is a value dependent on the detection platform, including the protocols and equipment used. Because the HCV concentration in the original commercial sample was stated to be  $2.5 \times 10^7$  IU/mL, the conversion factor from international units to copy number for HCV viral load in our test is approximately 0.9. The same conversion number (0.9) was published for the Roche Amplicor HCV Monitor v2.0 test when using a manual purification procedure.<sup>42</sup>

Table 1 summarizes the detection and quantification limits and dynamic range for the two multivolume SlipChip designs presented in this paper. Theory predicts that the dynamic range of design 1 can be easily extended by adding a set of wells smaller than 1 nL in volume and a set of wells larger than 125 nL in volume.<sup>34</sup> Therefore, if a larger dynamic range is required, the multiplexed design (design 2A) can be used for a single sample (design 2B). When using the entire chip for one sample, the 160 smallest wells (0.2 nL in volume) extend the upper limit of quantification with 3-fold resolution to  $2.0 \times 10^7$  molecules/mL in the RT-PCR mix and the 80 largest wells (625 nL in volume) extend the lower detection limit to 40 molecules/mL and lower dynamic range with 3-fold resolution to  $1.7 \times 10^2$  molecules/mL in the RT-PCR mix (Table 1, design 2B). This large dynamic range would be useful for quantification of viral load. A RT-PCR mix containing an HIV viral RNA sample (prepared as described above and then serially diluted) with an expected concentration of 51 molecules/mL was used to test the lower detection limit of design 2B (see Experimental Section in Supporting Information). We performed three negative control experiments (without HIV viral RNA) in parallel, and no false positives were observed. Six experiments were performed to quantify the viral RNA concentration (see Figure S1 in the Supporting Information for a representative experiment), and the average calculated HIV viral RNA concentration in the RT-PCR mix was 70 molecules/mL with standard deviation of 20 molecules/mL, corresponding to 32 molecules/mL with standard deviation of 9 molecules/mL in the original plasma sample.

To further validate the feasibility of using a rotational multivolume SlipChip to quantify HIV viral load, we used design 1 to measure HIV viral RNA purified from two archived samples of HIV-infected blood plasma from two different anonymous

patients. The HIV viral RNA from each patient sample was extracted and purified automatically using the iPrep purification instrument (see Experimental Section in Supporting Information), and concentrating factors of 7.1 and 6.6 were achieved for the two different patient samples. Each patient sample of purified HIV viral RNA was serially diluted and characterized by MV digital RT-PCR on the SlipChip using previously published primers,<sup>40</sup> and each experiment was repeated at least four times (Figure 6). The same plasma samples were characterized in a single experiment using the Roche COBAS AmpliPrep/COBAS TaqMan HIV-1 Test, v2.0 (CAP/CTM v2.0) according to the manufacturer's recommendation, and these values were treated as the standard for characterization. The data from SlipChip were self-consistent for both patients (Figure 6). Three negative control experiments using the same primers but no HIV template did not show false positive, as no increase of fluorescent intensity was observed (see Figure S2 in Supporting Information). For patient 1, the results (Figure 6, green crosses) were on average approximately 40% lower than that predicted by the single-point measurement of the HIV viral load using Roche CAP/CTM v2.0 (see Table S1 in Supporting Information). There were important differences in the test designs: while our experiment targets a single LTR region of HIV RNA, the Roche CAP/CTM v2.0 test includes two HIV sequences: one in *gag* and another in LTR region;<sup>43</sup> also, the two tests use different detection methods (EvaGreen in our experiment vs TaqMan probes in the Roche CAP/CTM v2.0 test) and different internal controls. Therefore, additional experiments with a large variety of patient samples from different virus subtypes are needed to further optimize and validate the multivolume approach to measuring viral load. For patient 2, excellent agreement with the Roche clinical measurement was observed over the entire range (Figure 6, red pluses, see also Table S2 in Supporting Information). This difference in agreement between the two methods for the two samples is not surprising, given that each patient has a unique HIV viral genome, and the primers, internal controls, and detection method used in one method may be better suited to detect one patient's viral genome than another's. Overall, taking into consideration the concentrating effect during sample preparation, the lowest concentration of serially diluted HIV viral RNA detected on the SlipChip corresponded to 37 molecules/mL in the patient plasma, and the highest concentration corresponded to 1.7 million molecules/mL in the patient plasma.

## CONCLUSIONS

Motivated by the problem of quantifying viral load under point-of-care and resource-limited settings, here we have successfully tested the applicability of multivolume digital assays<sup>34</sup> to quantitative analysis of RNA over wide dynamic range via digital RT-PCR on two rotational SlipChips (Table 1). The first chip has a dynamic range (at 95% CI) of  $5.2 \times 10^2$  to  $4.0 \times 10^6$  molecules/mL with 3-fold resolution and lower detection limit of  $1.2 \times 10^2$  molecules/mL. It was characterized using synthetic control RNA, demonstrating that MV digital RT-PCR performs in agreement with theoretical predictions<sup>34</sup> over the entire dynamic range (Figure 3). Results from wells of different volumes were mutually consistent and enabled quantification over a wide dynamic range using only 640 total wells (Figure 4). This chip was also validated with viral RNA from two HIV patients (Figure 6), demonstrating good agreement with single-point measurements performed on a Roche CAP/CTM v2.0 clinical instrument. Using

this chip, we were able to detect positive wells corresponding to a concentration of 81 molecules/mL HIV viral RNA purified from patient plasma in the RT-PCR mix, which corresponds to around 37 molecules/mL in the original plasma samples. While below the detection limit at 95% confidence interval, this concentration should give at least one positive well 86% of the time, so it is not surprising that all four of our experiments had at least one positive well at this concentration.

In the second chip, we tested the scalability and flexibility of the multivolume approach by introducing both multiplexed and higher-range quantification. We added additional wells with volumes of 0.2 nL and 625 nL and divided the SlipChip into five individual regions. We did not find evidence of cross-contamination among samples on this rotational design, in agreement with previous results on a translational SlipChip.<sup>31</sup> This multiplexed SlipChip was designed to test five samples, each at a dynamic range (3-fold resolution) from  $1.8 \times 10^3$  to  $1.2 \times 10^7$  molecules/mL with a lower detection limit of  $2.0 \times 10^2$  molecules/mL. Multiplexing capability (Figure 5) enables a number of features on the same chip, including (i) incorporating negative controls, (ii) measuring levels of control RNA to quantify the quality of sample preparation, (iii) monitoring coinfections, (iv) designing customized arrays for multiple targets, i.e. for nucleic acid targets that require measurements with different dynamic ranges and resolution, using wells of different sizes with customized numbers of wells at each size for each target, and (v) allowing for flexibility depending on technical and economic constraints by using the same device to perform either more analyses of lower quality, but at proportionally lower cost, or a single analysis of high quality including wider dynamic range and higher resolution. If this multiplexed SlipChip is used for a single sample, the dynamic range of the device with 3-fold resolution is designed to be  $1.7 \times 10^2$  to  $2.0 \times 10^7$  molecules/mL with a lower detection limit of 40 molecules/mL. Even with only a modest concentrating effect during sample preparation, this device would enable detecting targets at 10–20 molecules/mL in the original sample.

The high sensitivity of the this MV digital RT-PCR platform could be valuable for a number of applications beyond viral load, including detecting rare cells and rare mutations, prenatal diagnostics, and monitoring residual disease. Besides monitoring the HIV viral load of patients on antiretroviral treatments, this approach is also a promising method to screen newborns whose mothers are carrying HIV, where maternal HIV antibodies would potentially interfere with the antibody test. In addition, similar molecular diagnostics methods may be used to measure proviral DNA in infants. This approach can also be applied to investigation of copy number variation<sup>44,45</sup> and gene expression,<sup>46–48</sup> both for research and diagnostic settings.

The rotational format of SlipChip is attractive for resource-limited settings because the movement is easy to control even manually; for a chip with a 2 in. (50 mm) diameter an 8° rotation moves the outer edge of the chip by ~3.5 mm, a distance not difficult to move by hand especially with internal stoppers and guides. At the same time, it moves the wells which are 2.8 mm from the center by 0.39 mm. This feature is ideal for multivolume formats but also can be taken advantage of in single-volume formats. SlipChip is also particularly attractive for multivolume formats due to its lack of valves and ease of operation. A number of additional developments will increase the usefulness this chip. The trade-offs between resolution, dynamic range, and the extent of multiplexing of the multivolume SlipChip are described by theory<sup>34</sup> and can be mitigated by using different materials and

fabrication methods to increase the number of wells while keeping the footprint of the overall device the same. These improvements can come from deeper wells in two-layer devices or by creating multilayer devices. The designs characterized in this paper were fabricated in glass, and a functional SlipChip of a different design made from plastic by hot embossing was previously demonstrated.<sup>35</sup> For applications to resource-limited settings, devices made in inexpensive materials such as plastics would be desired.<sup>49</sup> These designs should be compatible with a number of sample preparation protocols being developed,<sup>50–52</sup> either integrated on-chip or performed off-chip. Additionally, the SlipChip would be compatible with other amplification chemistries that are currently being developed, such as polymerization and depolymerization methods,<sup>53–55</sup> toe-hold initiated hybridization-based amplification,<sup>56–58</sup> and other chemical amplifications including silver-based amplification.<sup>59,60</sup> When combined with isothermal amplification methods, such as recombinase polymerase amplification (RPA),<sup>33,61</sup> loop-mediated amplification (LAMP),<sup>62</sup> strand-displacement amplification (SDA),<sup>63</sup> helicase-dependent amplification (HDA),<sup>64</sup> and rolling circle amplification (RCA),<sup>65</sup> and visual readout methods, the MV digital RT-PCR SlipChip would make quantitative molecular diagnostics accessible in resource-limited settings.

## ASSOCIATED CONTENT

**Supporting Information.** Chemicals and materials, detailed experimental procedures, primer sequences, supplemental figures and tables. This material is available free of charge via the Internet at <http://pubs.acs.org>

## AUTHOR INFORMATION

### Corresponding Author

rustem.admin@caltech.edu

### Present Addresses

<sup>†</sup>SlipChip, LLC, 2201 Campbell Park Dr., Chicago, IL, 60612.

<sup>‡</sup>Department of Chemistry, Renmin University of China, Beijing, China, 100872.

<sup>§</sup>Division of Chemistry and Chemical Engineering, California Institute of Technology, 1200 E. California Blvd., Pasadena, CA 91125.

## ACKNOWLEDGMENT

This work was supported by NIH Grant No. 1R01 EB012946 administered by the National Institute of Biomedical Imaging and Bioengineering and by the NIH Director's Pioneer Award program, part of the NIH Roadmap for Medical Research (1 DP1 OD003584). We thank Heidi Park for contributions to writing and editing this manuscript. Disclosure: F.S. and R.F.I. have a financial interest in SlipChip LLC.

## REFERENCES

- Marcus, J. S.; Anderson, W. F.; Quake, S. R. *Anal. Chem.* **2006**, 78, 3084–3089.
- Stahlberg, A.; Bengtsson, M. *Methods* **2010**, 50, 282–288.
- Grond-Ginsbach, C.; Hummel, M.; Wiest, T.; Horstmann, S.; Pfleger, K.; Hergenhahn, M.; Hollstein, M.; Mansmann, U.; Grau, A. J.; Wagner, S. J. *Neurol.* **2008**, 255, 723–731.
- Kern, W.; Schoch, C.; Haferlach, T.; Schnittger, S. *Crit. Rev. Oncol./Hematol.* **2005**, 56, 283–309.
- Schmidt, U.; Fuessel, S.; Koch, R.; Baretton, G. B.; Lohse, A.; Tomasetti, S.; Unversucht, S.; Froehner, M.; Wirth, M. P.; Meye, A. *Prostate* **2006**, 66, 1521–1534.
- Anglicheau, D.; Suthanthiran, M. *Transplantation* **2008**, 86, 192–199.
- Whitney, J. B.; Luedemann, C.; Bao, S.; Miura, A.; Rao, S. S.; Mascola, J. R.; Letvin, N. L. *Aids* **2009**, 23, 1453–1460.
- Gurunathan, S.; El Habib, R.; Baglyos, L.; Meric, C.; Plotkin, S.; Dodet, B.; Corey, L.; Tartaglia, J. *Vaccine* **2009**, 27, 1997–2015.
- UNAIDS/WHO. 2008 Report on the Global AIDS Epidemic, 2008.
- Calmy, A.; Ford, N.; Hirschel, B.; Reynolds, S. J.; Lynen, L.; Goemaere, E.; de la Vega, F. G.; Perrin, L.; Rodriguez, W. *Clin. Infect. Dis.* **2007**, 44, 128–134.
- Shepard, C. W.; Finelli, L.; Alter, M. *Lancet Infect. Dis.* **2005**, 5, 558–567.
- US Food and Drug Administration. FDA approves Incivek for hepatitis C, 2011 <http://www.fda.gov/NewsEvents/Newsroom/PressAnnouncements/ucm256299.htm>.
- US Food and Drug Administration. FDA approves Victrelis for Hepatitis C, 2011 <http://www.fda.gov/NewsEvents/Newsroom/PressAnnouncements/ucm255390.htm>.
- Ferguson, M. C. *Pharmacotherapy* **2011**, 31, 92–111.
- Poordad, F.; et al. *New Engl. J. Med.* **2011**, 364, 1195–1206.
- Bustin, S. A. *Biomark. Med.* **2008**, 2, 201–207.
- Murphy, J.; Bustin, S. A. *Expert Rev. Mol. Diagn.* **2009**, 9, 187–197.
- Lee, H. H.; Dineva, M. A.; Chua, Y. L.; Ritchie, A. V.; Ushiro-Lumb, I.; Wisniewski, C. A. *J. Infect. Dis.* **2010**, 201, S65–S72.
- Department of Human Health and Human Services. Panel on Antiretroviral Guidelines for Adults and Adolescents. Guidelines for the use of antiretroviral agents in HIV-1-infected adults and adolescents, January 10, 2011 <http://www.aidsinfo.nih.gov/contentfiles/adultandadolescentgl.pdf>.
- World Health Organization. *Clinical and Laboratory Monitoring of Antiretroviral Therapy in Resource-Limited and Unlimited Settings*, 2000 <http://www.phclab.com/images/WHO%20Aids%20NI.pdf>.
- Sykes, P. J.; Neoh, S. H.; Brisco, M. J.; Hughes, E.; Condon, J.; Morley, A. *Biotechniques* **1992**, 13, 444–449.
- Vogelstein, B.; Kinzler, K. W. *Proc. Natl. Acad. Sci. U.S.A.* **1999**, 96, 9236–9241.
- Ottesen, E. A.; Hong, J. W.; Quake, S. R.; Leadbetter, J. R. *Science* **2006**, 314, 1464–1467.
- Fan, H. C.; Quake, S. R. *Anal. Chem.* **2007**, 79, 7576–7579.
- Beer, N. R.; Hindson, B. J.; Wheeler, E. K.; Hall, S. B.; Rose, K. A.; Kennedy, I. M.; Colston, B. W. *Anal. Chem.* **2007**, 79, 8471–8475.
- Leng, X. F.; Zhang, W. H.; Wang, C. M.; Cui, L. A.; Yang, C. J. *Lab Chip* **2010**, 10, 2841–2843.
- Pekin, D.; Skhiri, Y.; Baret, J.; Corre, D. L.; Mazutis, L.; Salem, C. B.; Millot, F.; Harrak, A. E.; Hutchison, J. B.; Larson, J. W.; Link, D. R.; Laurent-Puig, P.; Griffiths, A. D.; Taly, V. *Lab Chip* **2011**, 2156–2166.
- Sundberg, S. O.; Wittwer, C. T.; Gao, C.; Gale, B. K. *Anal. Chem.* **2010**, 82, 1546–1550.
- Applied Biosystems, Life Technologies. TaqMan® OpenArray® Digital PCR Plates, 2010 <https://products.appliedbiosystems.com/ab/en-US/adirect/ab?cmd=catNavigate2&catID=607965>.
- Du, W. B.; Li, L.; Nichols, K. P.; Ismagilov, R. F. *Lab Chip* **2009**, 9, 2286–2292.
- Shen, F.; Du, W. B.; Davydova, E. K.; Karymov, M. A.; Pandey, J.; Ismagilov, R. F. *Anal. Chem.* **2010**, 82, 4606–4612.
- Shen, F.; Du, W. B.; Kreutz, J. E.; Fok, A.; Ismagilov, R. F. *Lab Chip* **2010**, 10, 2666–2672.
- Shen, F.; Davydova, E. K.; Du, W. B.; Kreutz, J. E.; Piepenburg, O.; Ismagilov, R. F. *Anal. Chem.* **2011**, 83, 3533–3540.
- Kreutz, J. E.; Munson, T.; Huynh, T.; Shen, F.; Du, W.; Ismagilov, R. F. *Anal. Chem.* **2011**, DOI: 10.1021/ac201658s.
- Li, L. A.; Karymov, M. A.; Nichols, K. P.; Ismagilov, R. F. *Langmuir* **2010**, 26, 12465–12471.

- (36) Cochran, W. G. *Biometrics* **1950**, *6*, 105–116.
- (37) Destgroth, S. F. *J. Immunol. Methods* **1982**, *49*, R11–R23.
- (38) Halvorson, H. O.; Ziegler, N. R. *J. Bacteriol.* **1933**, *25*, 101–121.
- (39) Hurley, M. A.; Roscoe, M. E. *J. Appl. Bacteriol.* **1983**, *55*, 159–164.
- (40) McBreen, S.; Imlach, S.; Shirafuji, T.; Scott, G. R.; Leen, C.; Bell, J. E.; Simmonds, P. *J. Virol.* **2001**, *75*, 4091–4102.
- (41) Meng, S. A.; Li, J. M. *Virol. J.* **2010**, *7*, Article No: 117.
- (42) Pawlotsky, J. M. *Hepatology* **2002**, *36*, S65–S73.
- (43) Damond, F.; Avettand-Fenoel, V.; Collin, G.; Roquebert, B.; Plantier, J. C.; Ganon, A.; Sizmann, D.; Babiel, R.; Glaubitz, J.; Chaix, M. L.; Brun-Vezinet, F.; Descamps, D.; Rouzioux, C. **2010**, *48*, 1413–1416.
- (44) Qin, J.; Jones, R. C.; Ramakrishnan, R. *Nucleic Acids Res.* **2008**, *36*, Article No: e116.
- (45) Weaver, S.; Dube, S.; Mir, A.; Qin, J.; Sun, G.; Ramakrishnan, R.; Jones, R. C.; Livak, K. *J. Methods* **2010**, *50*, 271–276.
- (46) Warren, L.; Bryder, D.; Weissman, I. L.; Quake, S. R. *Proc. Natl. Acad. Sci. U.S.A.* **2006**, *103*, 17807–17812.
- (47) Winer, J.; Jung, C. K. S.; Shackel, I.; Williams, P. M. *Anal. Biochem.* **1999**, *270*, 41–49.
- (48) Zhao, J.; Moore, A. N.; Redell, J. B.; Dash, P. K. *J. Neurosci.* **2007**, *27*, 10240–10248.
- (49) Kuo, J. S.; Chiu, D. T. *Lab Chip* **2011**, *11*, 2656–2665.
- (50) Berry, S. M.; Alarid, E. T.; Beebe, D. J. *Lab Chip* **2011**, *11*, 1747–1753.
- (51) Jangam, S. R.; Yamada, D. H.; McFall, S. M.; Kelso, D. M. *J. Clin. Microbiol.* **2009**, *47*, 2363–2368.
- (52) Sur, K.; McFall, S. M.; Yeh, E. T.; Jangam, S. R.; Hayden, M. A.; Stroupe, S. D.; Kelso, D. M. *J. Molec. Diag.* **2010**, *12*, 620–628.
- (53) Sagi, A.; Weinstain, R.; Karton, N.; Shabat, D. *J. Am. Chem. Soc.* **2008**, *130*, S434–.
- (54) Sella, E.; Lubelski, A.; Klafter, J.; Shabat, D. *J. Am. Chem. Soc.* **2010**, *132*, 3945–3952.
- (55) Sikes, H. D.; Jenison, R.; Bowman, C. N. *Lab Chip* **2009**, *9*, 653–656.
- (56) Choi, H. M. T.; Chang, J. Y.; Trinh, L. A.; Padilla, J. E.; Fraser, S. E.; Pierce, N. A. *Nat. Biotechnol.* **2010**, *28*, 1208–U1103.
- (57) Zhang, D. Y.; Seelig, G. *Nat. Chem.* **2011**, *3*, 103–113.
- (58) Zhang, D. Y.; Turberfield, A. J.; Yurke, B.; Winfree, E. *Science* **2007**, *318*, 1121–1125.
- (59) Nam, J. M.; Thaxton, C. S.; Mirkin, C. A. *Science* **2003**, *301*, 1884–1886.
- (60) Taton, T. A.; Mirkin, C. A.; Letsinger, R. L. *Science* **2000**, *289*, 1757–1760.
- (61) Piepenburg, O.; Williams, C. H.; Stemple, D. L.; Armes, N. A. *PLoS Biol.* **2006**, *4*, 1115–1121.
- (62) Notomi, T.; Okayama, H.; Masubuchi, H.; Yonekawa, T.; Watanabe, K.; Amino, N.; Hase, T. *Nucleic Acids Res.* **2000**, *28*, Article No: e63.
- (63) Hellyer, T. J.; Nadeau, J. G. *Expert Rev. Mol. Diagn.* **2004**, *4*, 251–261.
- (64) Vincent, M.; Xu, Y.; Kong, H. M. *EMBO Rep.* **2004**, *5*, 795–800.
- (65) Lizardi, P. M.; Huang, X. H.; Zhu, Z. R.; Bray-Ward, P.; Thomas, D. C.; Ward, D. C. *Nat. Genet.* **1998**, *19*, 225–232.